

# A mean correction for improved phase-averaging accuracy in oscillatory, multiscale, differential equations

Timothy Charles Andrews\*      Beth A. Wingate\*

April 5, 2024

## Abstract

This paper introduces a new algorithm to improve the accuracy of numerical phase-averaging in oscillatory, multiscale, differential equations. Phase-averaging is a technique that applies averaging to a mapped variable to remove highly oscillatory linear terms from the differential equation. This retains the main contribution of fast oscillations on the low frequencies without needing to resolve the rapid oscillations themselves. However, this comes at the cost of an averaging error, which we aim to offset with a modified mapping. The new mapping includes a mean correction which encodes an average measure of the nonlinear interactions. This mapping was introduced in (Tao, 2019) for weak nonlinearity and relied on classical time averaging. Our algorithm extends this work to the case where 1) the nonlinearity is not weak but the linear oscillations are fast and 2) finite averaging windows are applied via a smooth kernel, which has the advantage of retaining low frequencies whilst still eliminating the fastest oscillations. We show that the new algorithm reduces phase errors in the mapped variable for the swinging spring ODE. We also demonstrate accuracy improvements compared to standard phase-averaging in numerical experiments with the one-dimensional Rotating Shallow Water Equations, a useful test case for weather and climate applications. As the mean correction term can be computed in parallel, this new mapping has potential as a more accurate, yet still computationally cheap, coarse propagator for the oscillatory parareal method.

## 1 Introduction

The ability to take larger timesteps, whilst retaining sufficient accuracy, is of great importance to reduce computational expense and time-to-solution. A particular motivation is weather and climate modelling, where the governing equations are highly oscillatory in nature. In previous decades, research into Semi-Lagrangian methods (Ritchie et al., 1995; Staniforth & Côté, 1991; Temperton & Staniforth, 1987) and Implicit-Explicit (IMEX) timesteppers (Bao et al., 2015; Giraldo et al., 2013; Weller et al., 2013) enabled larger timesteps for global weather forecasting models without sacrificing accuracy (Mengaldo et al., 2018). An alternative approach is the phase-averaging method. This has the potential for further reductions in time-to-solution through time parallelism (T. Haut & Wingate, 2014; Yamazaki et al., 2023). This paper proposes a new algorithm to improve the accuracy of this phase-averaging method.

---

\*University of Exeter (ta440@exeter.ac.uk, b.wingate@exeter.ac.uk)

Phase-averaging is a numerical technique that uses mapping and averaging to smooth out fast linear oscillations, whilst retaining the lower frequencies. First, a mapping to a modulation variable enables a time evolution without the leading-order oscillations, which can increase the allowable timestep size of explicit methods. Next, a phase-average of the modulation variable timestepping equation is applied to smooth the higher-order oscillations. This further reduces the numerical stiffness in the equations, but comes at the cost of introducing an averaging error. We seek to increase the accuracy of the phase-averaged method presented in (A. G. Peddle et al., 2019) by including a mean correction term, which encodes an average of the nonlinearity, into the modulation variable mapping. This technique was introduced by Tao in (Tao, 2019) for weakly nonlinear problems using classical averaging techniques (Sanders et al., 2007). Our algorithm in this paper can be considered a generalization of Tao’s method for the case when the equation is not weakly nonlinear, but oscillating and multiscale, and a finite averaging window is applied using a smooth kernel.

The advantage of using a finite averaging window for numerical phase averaging was discussed in detail in (A. Peddle, 2018). There it was shown that the error bound of this approach is a function of the timestep size,  $\Delta T$ , the averaging window,  $\eta$ , and a parameter,  $\epsilon$ , which represents the speed of the fast linear oscillations. The advantage of a finite phase-average is that the error bound not only holds in the limit of  $\epsilon$  small, as in classical averaging, but also for finite values of  $\epsilon$ .

We consider the application of phase-averaging to multiscale initial value problems of the form,

$$\frac{\partial \mathbf{u}}{\partial t} + \frac{1}{\epsilon} \mathcal{L} \mathbf{u} = \mathcal{N}(\mathbf{u}), \quad \mathbf{u}(0) = \mathbf{u}_0, \quad \epsilon \in (0, 1], \quad \epsilon \in \mathbb{R}, \quad (1)$$

where  $\mathbf{u}(t)$  is a (spatial) vector valued function,  $\mathbf{u}(t) = (u_1(t, \cdot), u_2(t, \cdot), \dots)$ ,  $\mathcal{L}$  has purely imaginary (oscillatory) eigenvalues, and  $\mathcal{N}(\mathbf{u})$  is an autonomous nonlinear term with arbitrary order polynomial components. In this paper we will consider (1) to be either an ODE, or a PDE that has been discretised in space to form a system of ODEs. The parameter  $\epsilon$ , which is assumed to be small, is a measure of how rapid the linear oscillations are. The need to sufficiently resolve the fastest of these frequencies on an  $\mathcal{O}(\epsilon^{-1})$  timescale constrains the maximum allowable timestep of explicit timestepping methods in (1). This restriction to small timesteps is true for implicit methods, too, if accuracy is required.

The phase-averaging approach firstly introduces a matrix exponential mapping to a ‘modulation’ variable. We define the modulation variable,  $\mathbf{v}$ , as,

$$\mathbf{u}(t) = e^{-\frac{t}{\epsilon} \mathcal{L}} \mathbf{v}(t), \quad (2)$$

which used in (1) leads to a new system to timestep,

$$\frac{\partial \mathbf{v}}{\partial t} = e^{\frac{t}{\epsilon} \mathcal{L}} \mathcal{N} \left( e^{-\frac{t}{\epsilon} \mathcal{L}} \mathbf{v} \right), \quad \mathbf{v}(0) = \mathbf{u}_0. \quad (3)$$

The original equation (1) can be recovered by applying the inverse of the matrix exponential to (3). Advantageously, the modulation variable system (3) has no linear terms oscillating on an  $\mathcal{O}(\epsilon^{-1})$  timescale. The use of mapping to a modulation variable equation is standard practice in the method of averaging (Bogoliubov & Mitropolsky, 1961; Sanders et al., 2007) and has been used to solve stiff PDEs in different fields, including optics (Hult, 2007) and geophysical fluid flows (Babin et al., 1997, 1998; Embid & Majda, 1998; Jones et al., 1999; Klainerman & Majda, 1981).

Taking another time-derivative of (3) shows there can still be oscillations in the higher derivatives. Therefore, phase-averaging is used to smooth these small amplitude oscillations, further

reducing the numerical stiffness. We facilitate this by introducing a phase variable,  $s$ , into the linear mapping of (2) to specify a time-translation, as in (Bauer et al., 2022; A. Peddle, 2018),

$$\mathbf{u}(t, s) = e^{-\frac{t+s}{\epsilon}\mathcal{L}}\mathbf{v}(t, s), \quad (4)$$

so that the phase variable appears in the timestepping equation (3),

$$\frac{\partial \mathbf{v}(t, s)}{\partial t} = e^{\frac{t+s}{\epsilon}\mathcal{L}}\mathcal{N}\left(e^{-\frac{t+s}{\epsilon}\mathcal{L}}\mathbf{v}\right), \quad \mathbf{v}(0) = \mathbf{u}_0. \quad (5)$$

We then integrate over this phase variable to compute an average, denoted as  $\langle \cdot \rangle_s$ , leaving only time-dependence in the phase-averaged modulation variable,

$$\frac{\partial \bar{\mathbf{v}}(t)}{\partial t} = \left\langle e^{\frac{t+s}{\epsilon}\mathcal{L}}\mathcal{N}\left(e^{-\frac{t+s}{\epsilon}\mathcal{L}}\bar{\mathbf{v}}\right) \right\rangle_s, \quad \bar{\mathbf{v}}(0) = \mathbf{u}_0. \quad (6)$$

The method of averaging has a long history and a review can be found in (Sanders et al., 2007). It has been used to obtain numerical solutions of oscillatory differential equations in many different forms (see (Tao, 2019) for an overview). It was first proposed to solve systems like (1) using a predictor-corrector type parallel-in-time method by (T. Haut & Wingate, 2014). Their phase-averaging was classical – over an infinite time window for the phase variable,  $s \in (-\infty, \infty)$ . In (A. G. Peddle et al., 2019) this was extended to the more physically relevant case of a finite oscillation speed,  $\epsilon$ . This phase-average is computed over only a few oscillations through a finite window length,  $\eta$ , with  $s \in (-\eta/2, \eta/2)$ . This algorithm has been further developed for use with a finite element implementation of the Rotating Shallow Water Equations (RSWEs) on the sphere (Yamazaki et al., 2023) and a multi-level parareal method that uses different averaging windows on each level (Rosemeier et al., 2022).

The error induced by the averaging is balanced with the reduced numerical stiffness which allows a larger timestep in the averaged system. This leads to the possibility of choosing an  $(\eta, \Delta t)$  pair that achieves a minimum error (A. Peddle, 2018) for a given  $\epsilon$ . Our new algorithm in this paper seeks to reduce this minimum error by introducing an additional term into the modulation variable mapping of (2). This new term quantifies a local mean of the oscillations in the modulation variable space. This extension to the mapping ensures that less information is lost when phase-averaging the modulation variable equation (5). Further intuition around accuracy improvements are presented in (Tao, 2019) by considering the case when  $\mathcal{N}$  in (3) is a constant. The addition of a mean correction to the mapping can be considered an alternative to (Bauer et al., 2022), where higher-order versions of the phase-averaging are instead used to improve the accuracy.

For our new method investigated in this paper, we define a modified mapping to a different modulation variable,  $\mathbf{w}$ ,

$$\mathbf{u}(t, s) = e^{-\frac{t+s}{\epsilon}\mathcal{L}}\mathbf{w}(t, s) + \epsilon\mathcal{L}^{-1}\mathbf{C}, \quad (7)$$

where we have introduced the phase variable  $s$  into the explicit time-dependent part of the mapping to generalise that given in (Tao, 2019). Averaging over  $s$  gives,

$$\begin{aligned} \frac{\partial \bar{\mathbf{w}}(t)}{\partial t} &= \left\langle e^{\frac{t+s}{\epsilon}\mathcal{L}} \left[ \mathcal{N}\left(e^{-\frac{t+s}{\epsilon}\mathcal{L}}\bar{\mathbf{w}}(t) + \epsilon\mathcal{L}^{-1}\mathbf{C}\right) - \mathcal{L}\mathcal{L}^{-1}\mathbf{C} \right] \right\rangle_s, \\ \bar{\mathbf{w}}(0) &= \mathbf{u}_0 - \epsilon\mathcal{L}^{-1}\mathbf{C}(\bar{\mathbf{w}}(0)). \end{aligned} \quad (8)$$

In this paper we explore potential accuracy improvements of using (8) over (6). Section 2 delves into the phase-averaged and mean corrected methods, including pseudocode for the new algorithm.

We then explore the potential accuracy improvements of the new algorithm in three systems (sections 3-5). Section 3 presents the swinging spring ODE (Holm & Lynch, 2002) and uses an analytical mean correction to demonstrate its effect. The first PDE example in section 4 is a Klein-Gordon-type (KG-type) PDE, which is both weakly nonlinear and multiscale. Section 5 explores accuracy improvements in the one-dimensional Rotating Shallow Water Equations (RSWEs), a prototype PDE for those used in weather and climate applications. We demonstrate that the mean correction enables greater accuracy given sufficiently fast oscillations. In section 6 we discuss future improvements that can be made to the algorithm and method, and list further applications that could be investigated.

## 2 Phase-averaging and the mean correction

### 2.1 Improved accuracy for classical averaging

The original application of a mean correction with a modulation variable mapping was for a weakly nonlinear system (Tao, 2019),

$$\frac{\partial \mathbf{u}}{\partial \tau} + \mathcal{L}\mathbf{u} = \epsilon \mathcal{N}(\mathbf{u}). \quad (9)$$

For equations of type (9), Theorem 2 of (Tao, 2019) shows that the new mapping with the mean correction will perform no worse than the original modulation variable method, in the case of a classical time average. This was proved by setting  $F$  and  $G$  as the right-hand sides of the modulation variable and mean corrected timestepping equations without averaging, with  $\bar{F}$  and  $\bar{G}$  being the classically time averaged counterparts:

$$\begin{aligned} F &= e^{t\mathcal{L}}\mathcal{N}, \quad \bar{F} = \langle e^{t\mathcal{L}}\mathcal{N} \rangle_{\infty}, \\ G &= e^{t\mathcal{L}}(\mathcal{N} - \mathcal{L}\mathcal{L}^{-1}\mathbf{C}_{\infty}), \quad \bar{G} = \langle e^{t\mathcal{L}}(\mathcal{N} - \mathcal{L}\mathcal{L}^{-1}\mathbf{C}_{\infty}) \rangle_{\infty}, \end{aligned} \quad (10)$$

where the  $\infty$  subscript denotes integration over all time for a classical time average. The difference due to averaging in each system is  $\Delta F = F - \bar{F}$  and  $\Delta G = G - \bar{G}$ . Tao shows that  $\|\Delta G(x)\| \leq \|\Delta F(x)\|$ , for any  $x$ , until at least a time of  $t = \mathcal{O}(\epsilon^{-1})$ . As the averaging error in the mean corrected system is less than or equal to that in the classically averaged modulation variable system, there is the potential for accuracy improvements.

As is standard in the method of averaging, a change of variable to a slower timescale  $t = \epsilon\tau$ , provides a scaling between the multiscale (1) and weakly nonlinear (9) systems. As such, this result for a weakly nonlinear system on a  $\mathcal{O}(\epsilon^{-1})$  timescale will hold for a  $\mathcal{O}(1)$  timescale in systems of type (1). This motivates our extension of Tao's method for timestepping multiscale equations. The remainder of this section will highlight two key adaptations to the method of (Tao, 2019) for our use in multiscale equations: i) a finite phase-average is used instead of a classical time average (section 2.2), and ii) a 'numerical' mean correction using a finite time interval,  $\mathbf{C}$ , can be used instead of a classically time averaged  $\mathbf{C}_{\infty}$  (section 2.3).

### 2.2 Discussion of phase-averaging

Finite phase-averaging differs from a classical time average in that it is computed over a select number of oscillations. The phase-averaging technique introduces a dummy phase variable,  $s$ , into the linear mapping, and integrates over this variable with respect to a weighted kernel function.

The range of phase shifts used in the average are those contained within the averaging window of length  $\eta$ . We define the  $\langle \cdot \rangle_s$  average as,

$$\langle \phi \rangle_s = \int_{s=-\eta/2}^{\eta/2} \mathcal{K}(s) \phi \, ds, \quad (11)$$

where  $\mathcal{K}(s)$  denotes the averaging kernel function. Substituting this into (8) obtains:

$$\frac{\partial \bar{\mathbf{v}}(t)}{\partial t} = \int_{s=-\eta/2}^{\eta/2} \mathcal{K}(s) e^{\frac{t+s}{\epsilon} \mathcal{L}} \mathcal{N} \left( e^{-\frac{t+s}{\epsilon} \mathcal{L}} \bar{\mathbf{v}}(t) \right) ds. \quad (12)$$

This approach of numerical averaging with a kernel is analogous to forming the ‘effective’ system in Heterogeneous Multiscale Methods (Engquist & Tsai, 2005).

There are three regimes of averaging window length that could be used in (12) — case iii) is of specific interest in this paper:

- i) The limit of  $\eta = 0$  implies no averaging, returning to the standard modulation variable system of (3). This equation remains constrained by small amplitude oscillations.
- ii) The other limit as  $\eta \rightarrow \infty$  simulates the limit of  $\epsilon \rightarrow 0$ . This solution has a complete cancellation of oscillations; any parts of the solution with periodicity, and thus phase dependence, are driven to zero. As such, only non-oscillatory components provide a contribution to the leading-order solution (Schochet, 1992). (T. Haut & Wingate, 2014) showed that the dynamics in this limit can be replicated with a sufficiently large  $\eta$ .
- iii) A averaging window with minimum error,  $\eta^*$ , was shown to exist in finite ( $\epsilon$ ) regimes (A. G. Peddle et al., 2019). Insufficient averaging ( $\eta < \eta^*$ ) means that the timestepping equations remain too stiff, which leaves a significant timestepping error. Excessive averaging ( $\eta > \eta^*$ ) removes dynamical information contained in the oscillations, so the averaging error dominates. The combination of timestepping error (decreasing with  $\eta$ ) and averaging error (increasing with  $\eta$ ) is smallest at the minimum averaging window,  $\eta^*$ . Visualisations of phase-averaged solution errors against  $\eta$ , in order to identify  $\eta^*$ , will be termed ‘Peddle plots’ (see Figure 2 for an example in the swinging spring ODE, or the thesis of Adam Peddle (A. Peddle, 2018) for others). As  $\eta^*$  depends on the timestep size, errors are computed over a range of normalised averaging windows,  $\zeta = \eta/\Delta t$ .

An exponential bump kernel is selected to ensure sufficient smoothness when approximating the  $\epsilon \rightarrow 0$  limit with a compact support (T. Haut & Wingate, 2014). The kernel has a maximum value at no phase shift ( $s = 0$ ) and decays to zero at the boundaries of the averaging interval,

$$\mathcal{K}(s) = \begin{cases} A \exp\left(\frac{-\eta}{\alpha(0.5\eta+s)(0.5\eta-s)}\right), & s \in \left(-\frac{\eta}{2}, \frac{\eta}{2}\right), \\ 0, & |s| \geq \frac{\eta}{2}, \end{cases} \quad (13)$$

where  $A$  is a normalisation constant to ensure that  $\int_{s=-\infty}^{\infty} \mathcal{K}(s) \, ds = 1$ . A kernel decay rate,  $\alpha$ , controls the shape of the exponential over the compact support. Values of  $\alpha = 1$  (A. G. Peddle et al., 2019; Yamazaki et al., 2023) and  $\alpha = 4$  (A. Peddle, 2018) have been used in prior applications — we use the latter for the results in this paper.

The numerical implementation can be expressed as a sum of evaluations at  $K$  equispaced phase shifts,

$$\frac{\partial \bar{\mathbf{v}}(t)}{\partial t} = \sum_{k=1}^K \mathcal{K}(s_k) e^{\frac{t+s_k}{\epsilon} \mathcal{L}} \mathcal{N} \left( e^{-\frac{t+s_k}{\epsilon} \mathcal{L}} \bar{\mathbf{v}}(t) \right), \quad s_k = \left( \frac{2k-1}{2K} - \frac{1}{2} \right) \eta, \quad (14)$$

where the discrete kernel values are normalised to ensure that  $\sum_{k=1}^K \mathcal{K}(s_k) = 1$ .

Convergence of the numerical phase-average requires a sufficient number of discrete kernel points,  $K$ . For PDE systems, this scales with the fastest resolvable frequency and averaging window length. The following rule is used to compute  $K$ ,

$$K = \left\lceil P \eta \frac{\omega_{max}}{2\pi\epsilon} \right\rceil, \quad (15)$$

where  $\lceil \cdot \rceil$  denotes the ceiling function,  $\omega_{max}$  is fastest resolvable frequency of  $\mathcal{L}$ , and  $P$  is the number of samples within each period of this fastest frequency. To have sufficient sampling of the fastest oscillations, a value of at least  $P = 3.5$  is recommended for pseudospectral methods (Boyd, 2001). We use  $P = 4$ , as was used for sufficient convergence for phase-averaging in (Yamazaki et al., 2023). As a proportionally larger number of points per oscillation may be required when sampling fewer oscillations (Boyd, 2001), a minimum  $K$  value is also specified.

A key feature of the phase-average in (12) is that fluctuations in the matrix exponential are averaged at a *fixed* value of the solution,  $\bar{\mathbf{v}}(t)$ . This only requires phase-shifting the deterministic oscillations contained in the linear operator,  $\mathcal{L}$ . As the computations at each  $s$  value have no feedback on each other, the phase-average can be computed in parallel (Yamazaki et al., 2023).

### 2.3 The mean corrected method

The new algorithm for improved accuracy computes a mean correction term,  $\mathbf{C}$ , and incorporates this into a new mapping (7).  $\mathbf{C}$  quantifies an average value of the effect of nonlinear oscillations of the modulation variable,

$$\mathbf{C} = \left\langle \mathcal{N} \left( e^{-\frac{t+r}{\epsilon} \mathcal{L}} \mathbf{w}(t) \right) \right\rangle_r, \quad (16)$$

where  $r$  is an analogous phase variable to  $s$  and  $\langle \cdot \rangle_r$  denotes the averaging operation to compute the mean correction.

The mean correction application in (Tao, 2019) used a classical time average for the mean correction,

$$\mathbf{C}_\infty(\mathbf{w}(t)) = \lim_{T_C \rightarrow \infty} \frac{1}{T_C} \int_{r=0}^{T_C} \mathcal{N} \left( e^{-\frac{t+r}{\epsilon} \mathcal{L}} \mathbf{w}(t) \right) dr. \quad (17)$$

In some situations, it is feasible to compute a closed-form expression for  $\mathbf{C}_\infty$  using (17); we call this an ‘analytical’ mean correction. An analytical mean correction will be used in the ODE system of the swinging spring, (section 3), as well as the KG-type system (section 4), which is possible due to our use of a pseudospectral method throughout this work. More generally, a closed-form expression cannot be derived, so a ‘numerical’ mean correction is used instead. This is computed using an analogous phase-averaging computation for  $\langle \cdot \rangle_r$  as is used for  $\langle \cdot \rangle_s$ ,

$$\mathbf{C}(\mathbf{w}(t), t) = \int_{r=-\eta_C/2}^{\eta_C/2} \mathcal{K}_C(r) \mathcal{N} \left( e^{-\frac{t+r}{\epsilon} \mathcal{L}} \mathbf{w}(t) \right) dr, \quad (18)$$

where  $\mathcal{K}_C$  is the mean correction averaging kernel of length  $\eta_C$ . We select the same functional form for  $\mathcal{K}_C(r)$  as is defined for  $\mathcal{K}(s)$  in (13). The required  $K_s$  number of points in the mean correction

kernel is computed using (15) with  $\eta_C$  in place of  $\eta$ . A numerical mean correction can be computed irrespective of the spatial discretisation choice and is given in algorithm 1.

---

**Algorithm 1** The Numerical Mean Correction

---

Numerical\_C( $\mathbf{w}^n, t^n$ ) :

- 1: **parfor**  $k \in \{1, 2, \dots, K_s\}$  **do**
  - 2:      $\mathbf{u}_k \leftarrow \exp(-((t^n + r_k)/\epsilon)\mathcal{L})\mathbf{w}^n$
  - 3:      $\mathcal{N}_k \leftarrow \mathcal{N}(\mathbf{u}_k)$
  - 4: **end parfor**
  - 5:  $\mathbf{C} \leftarrow \sum_{k=1}^{K_s} \mathcal{K}_C(k)\mathcal{N}_k$
  - 6: **Return**  $\mathbf{C}$
- 

As with the  $\langle \cdot \rangle_s$  phase-averaging procedure, the numerical mean correction of  $\langle \cdot \rangle_r$  is computed at a fixed solution state,  $\mathbf{w}(t)$ , so is parallelisable. The numerically mean corrected method requires selecting a suitable window pairing of  $(\eta, \eta_C)$ . Analogously to an  $\eta^*$  minimising the error of the  $\langle \cdot \rangle_s$  phase-average, the existence of a finite  $\eta_C^*$  which minimises the error of the numerically mean corrected method is demonstrated in sections 4 and 5. Specific choices for the  $(\eta, \eta_C)$  pairing in the KG-type and RSWEs systems are described in their respective sections.

We now apply this new modulation variable transformation (7), using either the analytical or numerical mean correction, to the standard form equation (1),

$$\begin{aligned} & \frac{\partial}{\partial t} \left( e^{-\frac{t+s}{\epsilon}\mathcal{L}}\mathbf{w} + \epsilon\mathcal{L}^{-1}\mathbf{C} \right) + \frac{1}{\epsilon}\mathcal{L} \left( e^{-\frac{t+s}{\epsilon}\mathcal{L}}\mathbf{w} + \epsilon\mathcal{L}^{-1}\mathbf{C} \right) = \mathcal{N}, \\ \rightarrow & -\frac{1}{\epsilon}\mathcal{L}e^{-\frac{t+s}{\epsilon}\mathcal{L}}\mathbf{w} + e^{-\frac{t+s}{\epsilon}\mathcal{L}}\frac{\partial\mathbf{w}}{\partial t} + \epsilon\frac{\partial}{\partial t}(\mathcal{L}^{-1}\mathbf{C}) + \frac{1}{\epsilon}\mathcal{L}e^{-\frac{t+s}{\epsilon}\mathcal{L}}\mathbf{w} + \mathcal{L}\mathcal{L}^{-1}\mathbf{C} = \mathcal{N}, \\ \rightarrow & e^{-\frac{t+s}{\epsilon}\mathcal{L}}\frac{\partial\mathbf{w}}{\partial t} + \epsilon\frac{\partial}{\partial t}(\mathcal{L}^{-1}\mathbf{C}) = \mathcal{N} - \mathcal{L}\mathcal{L}^{-1}\mathbf{C}. \end{aligned}$$

Applying the chain rule to the  $\epsilon\frac{\partial}{\partial t}(\mathcal{L}^{-1}\mathbf{C})$  term,

$$\left( e^{-\frac{t+s}{\epsilon}\mathcal{L}} + \epsilon\frac{\partial}{\partial\mathbf{w}}(\mathcal{L}^{-1}\mathbf{C}) \right) \frac{\partial\mathbf{w}}{\partial t} = \mathcal{N} - \mathcal{L}\mathcal{L}^{-1}\mathbf{C}. \quad (19)$$

Following (Tao, 2019) we assume that the  $\epsilon\frac{\partial}{\partial\mathbf{w}}(\mathcal{L}^{-1}\mathbf{C})$  term can be neglected at  $\mathcal{O}(1)$ . This leaves the following time-evolution equation for the mean corrected modulation variable,

$$\frac{\partial\mathbf{w}(t, s)}{\partial t} = e^{\frac{t+s}{\epsilon}\mathcal{L}} \left[ \mathcal{N} \left( e^{-\frac{t+s}{\epsilon}\mathcal{L}}\mathbf{w} + \epsilon\mathcal{L}^{-1}\mathbf{C} \right) - \mathcal{L}\mathcal{L}^{-1}\mathbf{C} \right]. \quad (20)$$

This equation is phase-averaged over a finite time window to give the following numerical system for  $\bar{\mathbf{w}}$ ,

$$\begin{aligned} \frac{\partial\bar{\mathbf{w}}(t)}{\partial t} &= \int_{s=-\eta/2}^{\eta/2} \mathcal{K}(s)e^{\frac{t+s}{\epsilon}\mathcal{L}} \left[ \mathcal{N} \left( e^{-\frac{t+s}{\epsilon}\mathcal{L}}\bar{\mathbf{w}} + \epsilon\mathcal{L}^{-1}\mathbf{C} \right) - \mathcal{L}\mathcal{L}^{-1}\mathbf{C} \right] ds, \\ \bar{\mathbf{w}}(0) &= \mathbf{u}_0 - \epsilon\mathcal{L}^{-1}\mathbf{C}(\bar{\mathbf{w}}(0)). \end{aligned} \quad (21)$$

The new algorithm that solves (21) is given in algorithm 2. This is presented in a format where the averaging procedures of  $\langle \cdot \rangle_s$  and  $\langle \cdot \rangle_r$  can be computed in parallel (using parfor). As this

paper is mainly concerned with exploring potential accuracy improvements, not parallelisation, we present results that use a serial implementation.

Many systems have non-singular linear matrices, so the  $-\mathcal{L}\mathcal{L}^{-1}\mathbf{C}$  term in (21) often simplifies to  $-\mathbf{C}$ . However, this reduction does not occur in some systems, including the RSWEs of section 5. When  $\mathcal{L}^{-1}$  is undefined, a Moore-Penrose pseudoinverse (Penrose, 1955),  $\mathcal{L}^+$ , is used instead, as suggested by Tao in (Tao, 2019).

It is important to note that the initial condition for the modulation variable in (21) is defined implicitly. This can be cheaply computed using a fixed-point iteration, given in algorithm 3, starting from a guess of  $\mathbf{w}_0 = \mathbf{u}_0$ . This implicit equation only needs to be solved once, as after the initial condition in the  $\mathbf{w}$  space is found, an explicit timestepping scheme is applied as per standard phase-averaging.

---

**Algorithm 2** The Mean Corrected Method

---

We present the algorithm in terms of Butcher tableau coefficients  $a_{ij}, b_i, c_i$  for a general explicit Runge-Kutta scheme (Butcher, 2016), i.e. classical RK4.

- 1: Using the standard initial condition,  $\mathbf{u}_0$ , compute the initial mean correction,  $\mathbf{C}_0$ , and the initial mean corrected modulation variable,  $\mathbf{w}_0$ . This usually requires iteration (algorithm 3).
  - 2: **for** each timestep **do**
  - 3:      $\mathbf{C}_1 \leftarrow \mathbf{C}_0$
  - 4:      $\mathbf{w}_1 \leftarrow \mathbf{w}_0$
  - 5:     Compute  $\mathbf{w}^{n+1}$  from the current time solution,  $\mathbf{w}^n$ , using phase-averaged function evaluations,  $\bar{\mathbf{f}}_i(\mathbf{w}_i, t_i)$ , for the  $M$  intermediate steps i.e.  $M = 4$  for RK4.
  - 6:     **for**  $i \in \{1, \dots, M\}$  **do**
  - 7:          $t_i \leftarrow t^n + c_i \Delta t$
  - 8:         **if**  $i \neq 1$  **then**
  - 9:              $\mathbf{C}_i \leftarrow \mathbf{C}(\mathbf{w}_i, t_i)$  (Use algorithm 1 for a numerical mean correction)
  - 10:         **end if**
  - 11:         **parfor**  $k \in \{1, 2, \dots, K\}$  **do**
  - 12:              $\mathbf{u}_k \leftarrow \exp(-((t_i + s_k)/\epsilon)\mathcal{L})\mathbf{w}_i + \epsilon\mathcal{L}^{-1}\mathbf{C}_i$
  - 13:              $\mathcal{N}_k \leftarrow \mathcal{N}(\mathbf{u}_k)$
  - 14:              $\mathbf{f}_k \leftarrow \exp(((t_i + s_k)/\epsilon)\mathcal{L})[\mathcal{N}_k - \mathcal{L}\mathcal{L}^{-1}\mathbf{C}_i]$
  - 15:         **end parfor**
  - 16:          $\bar{\mathbf{f}}_i \leftarrow \sum_{k=1}^K \mathcal{K}(s_k)\mathbf{f}_k$
  - 17:         **if**  $i \neq M$  **then**
  - 18:              $\mathbf{w}_{i+1} = \mathbf{w}^n + \Delta t \sum_{j=1}^i a_{i+1,j} \bar{\mathbf{f}}_j$
  - 19:         **end if**
  - 20:     **end for**
  - 21:      $\mathbf{w}^{n+1} = \mathbf{w}^n + \Delta t \sum_{i=1}^M b_i \bar{\mathbf{f}}_i$
  - 22:      $\mathbf{w}_0 \leftarrow \mathbf{w}^{n+1}$
  - 23:      $\mathbf{C}_0 \leftarrow \mathbf{C}(\mathbf{w}^{n+1}, t^{n+1})$
  - 24:     Back-transform to the standard variable solution at timepoints of interest:
  - 25:      $\mathbf{u}^{n+1} = \exp(-(t^{n+1}/\epsilon)\mathcal{L})\mathbf{w}^{n+1} + \epsilon\mathcal{L}^{-1}\mathbf{C}_0$
  - 26: **end for**
  - 27: Return all values of  $\mathbf{u}, \mathbf{w}$
-



---

**Algorithm 3** Fixed-point iteration for computing  $\mathbf{w}(0)$ 

---

$\mathbf{w0\_iteration}(\mathbf{u}_0, C_{tol})$ :

- 1:  $\mathbf{C}_0 \leftarrow \mathbf{C}(\mathbf{u}_0, 0)$
  - 2:  $\mathbf{w}_0 \leftarrow \mathbf{u}_0 - \epsilon \mathcal{L}^{-1} \mathbf{C}_0$
  - 3:  $\mathbf{C}_{new} \leftarrow \mathbf{C}(\mathbf{w}_0, 0)$
  - 4: **while**  $\sum |\mathbf{C}_0 - \mathbf{C}_{new}| > C_{tol}$  **do**
  - 5:      $\mathbf{C}_0 \leftarrow \mathbf{C}_{new}$
  - 6:      $\mathbf{w}_0 \leftarrow \mathbf{u}_0 - \epsilon \mathcal{L}^{-1} \mathbf{C}_0$
  - 7:      $\mathbf{C}_{new} \leftarrow \mathbf{C}(\mathbf{w}_0, 0)$
  - 8: **end while**
  - 9:  $\mathbf{C}_0 \leftarrow \mathbf{C}_{new}$
  - 10: Return  $\mathbf{w}_0, \mathbf{C}_0$
- 

### 3 ODE Example: The Swinging Spring

The first numerical example is the swinging spring ODE. This models a point mass attached to a spring, enabling vertical oscillations in addition to the typical, pendulum, motion. Two distinct physical normal modes, of swinging (with a frequency of  $\omega_R$ ) and elastic springing (with a frequency of  $\omega_Z$ ) exhibit fast, oscillatory, dynamics. These fast modes also interact to construct a slow timescale stepwise precession, where the angle of the pendulum position in the  $x - y$  plane has large shifts in value at certain times (Holm & Lynch, 2002). One full cycle of the nonlinear phase precession occurs on a slower timescale than the swinging and springing modes, corresponding to  $\epsilon \approx 0.01$  (Bauer et al., 2022).

The presence of multiple timescales in the swinging spring intentionally mimics weather and climate models, i.e. the separation of fast inertia-gravity waves and slow Rossby waves of the RSWEs (Lynch, 2003). A considerable volume of literature has analysed a 2:1 resonance between the swinging and springing modes to mimic a directly resonant interaction of the linear waves, e.g. (Dullin et al., 2004; Holm & Lynch, 2002; Lynch, 2002), and with higher-order phase-averaging in (Bauer et al., 2022). In preparation for the PDE systems, which contain a spectrum of in- and out- of resonance interactions, we examine the swinging spring over a wider range of dynamical scenarios. Introducing a ‘resonance factor’ as a ratio of the two normal mode frequencies,  $\rho = \omega_Z/\omega_R$ , we examine the range of interactions,  $\rho \in [1.5, 2.5]$ . This includes out-of-resonance (e.g.  $\rho = 1.5$ ) and near-resonance (e.g.  $\rho = 1.95$ ) interactions, as well as the 2:1 directly resonant scenario ( $\rho = 2$ ).

#### 3.1 Equations

We use the governing equations in (Holm & Lynch, 2002), which were derived using a cubic-order truncated Lagrangian for the pendulum’s position as a function of time,

$$\frac{d^2 x}{dt^2} + \omega_R^2 x = \lambda x z, \tag{22a}$$

$$\frac{d^2 y}{dt^2} + \omega_R^2 y = \lambda y z, \tag{22b}$$

$$\frac{d^2 z}{dt^2} + \omega_Z^2 z = \frac{\lambda}{2}(x^2 + y^2), \tag{22c}$$

where  $\omega_R = \sqrt{g/l}$ ,  $\omega_Z = \sqrt{k/m}$ ,  $\lambda = l_o\omega_Z^2/l^2$ , and  $l, l_o$  are the equilibrium and unstretched spring lengths respectively.

Following (Bauer et al., 2022), the following transformation is applied to form a first-order system in time; it also simplifies the linear, Skew-Hermitian, operator,

$$\frac{dx}{dt} = \omega_R p_x, \quad \frac{dy}{dt} = \omega_R p_y, \quad \frac{dz}{dt} = \omega_Z p_z, \quad (23)$$

where  $p_a := \frac{\partial p}{\partial a}$ ,  $a \in \{x, y, z\}$ .

Complex variables, denoted with a hat, are introduced so that the solution vector,  $\mathbf{u} = [\hat{x}, \hat{y}, \hat{z}]^T$ , contains three variables instead of six,

$$\hat{x} = x + ip_x, \quad \hat{y} = y + ip_y, \quad \hat{z} = z + ip_z. \quad (24)$$

Taking the real part,  $\Re()$ , of each component of  $\mathbf{u}$  recovers the position in that coordinate. Using the resonance factor,  $\rho = \omega_Z/\omega_R$ , to relate the swinging and springing modes, we arrive at an equation for  $\mathbf{u} = [\hat{x}, \hat{y}, \hat{z}]^T$  in the standard form of (1). Although  $\epsilon$  is not explicitly shown in the swinging spring system (so  $\epsilon = 1$  is used with algorithm 2) it is intrinsically part of the multiscale dynamics ( $\epsilon \approx 0.01$ ) (Bauer et al., 2022). In this standard form, the linear and nonlinear operators are,

$$\mathcal{L} = \begin{bmatrix} i\omega_R & 0 & 0 \\ 0 & i\omega_R & 0 \\ 0 & 0 & i\rho\omega_R \end{bmatrix}, \quad \mathcal{L}^{-1} = \begin{bmatrix} \frac{-i}{\omega_R} & 0 & 0 \\ 0 & \frac{-i}{\omega_R} & 0 \\ 0 & 0 & \frac{-i}{\rho\omega_R} \end{bmatrix}, \quad \mathcal{N} = \begin{bmatrix} \frac{i\lambda}{\omega_R} \Re(\hat{x})\Re(\hat{z}) \\ \frac{i\lambda}{\omega_R} \Re(\hat{y})\Re(\hat{z}) \\ \frac{i\lambda}{2\rho\omega_R} [\Re(\hat{x})^2 + \Re(\hat{y})^2] \end{bmatrix}. \quad (25)$$

Because  $\mathcal{L}$  is a diagonal matrix, the matrix exponential is simply the exponentiation of the nonzero elements,

$$e^{\pm t\mathcal{L}} = \begin{bmatrix} e^{\pm i\omega_R t} & 0 & 0 \\ 0 & e^{\pm i\omega_R t} & 0 \\ 0 & 0 & e^{\pm i\rho\omega_R t} \end{bmatrix}. \quad (26)$$

### 3.2 An Analytical Mean Correction

As a first demonstration of the mean corrected method, we use an analytical mean correction corresponding to (17). Consider the nonlinear vector in terms of the mean corrected modulation variable,  $\mathbf{w} = [\tilde{x}, \tilde{y}, \tilde{z}]^T$ ,

$$\mathcal{N}(e^{-t\mathcal{L}}\mathbf{w}) = \begin{bmatrix} \frac{i\lambda}{\omega_R} \Re(e^{-i\omega_R t}\tilde{x})\Re(e^{-i\rho\omega_R t}\tilde{z}) \\ \frac{i\lambda}{\omega_R} \Re(e^{-i\omega_R t}\tilde{y})\Re(e^{-i\rho\omega_R t}\tilde{z}) \\ \frac{i\lambda}{2\rho\omega_R} [\Re(e^{-i\omega_R t}\tilde{x})^2 + \Re(e^{-i\omega_R t}\tilde{y})^2] \end{bmatrix}. \quad (27)$$

Using that  $\Re(AB) = (1/2)(AB + A^*B^*)$ , where the  $*$  denotes complex conjugation,

$$\mathcal{N}(e^{-t\mathcal{L}}\mathbf{w}) = \begin{bmatrix} \frac{i\lambda}{4\omega_R} (A\tilde{x}\tilde{z} + B\tilde{x}\tilde{z}^* + C\tilde{x}^*\tilde{z} + D\tilde{x}^*\tilde{z}^*) \\ \frac{i\lambda}{4\omega_R} (A\tilde{y}\tilde{z} + B\tilde{y}\tilde{z}^* + C\tilde{y}^*\tilde{z} + D\tilde{y}^*\tilde{z}^*) \\ \frac{i\lambda}{8\rho\omega_R} (E(\tilde{x}^2 + \tilde{y}^2) + 2(\tilde{x}\tilde{x}^* + \tilde{y}\tilde{y}^*) + F(\tilde{x}^{*2} + \tilde{y}^{*2})) \end{bmatrix}, \quad (28)$$

where,

$$A = e^{-i(\rho+1)\omega_R t}, \quad B = e^{i(\rho-1)\omega_R t}, \quad C = e^{-i(\rho-1)\omega_R t}, \\ D = e^{i(\rho+1)\omega_R t}, \quad E = e^{-2i\omega_R t}, \quad F = e^{2i\omega_R t}.$$

For the range of resonance factors considered, all the complex exponential terms ( $A$  to  $F$ ) will have a nonzero argument. A cancellation of oscillations occurs when computing  $\langle \cdot \rangle_r$  in the classical limit of  $r \rightarrow \infty$ , so that each of these terms has a zero mean value (refer to Appendix A for a demonstration of this). As a result, the only nonzero term is in the  $z$  coordinate,

$$\mathbf{C}_\infty = \begin{bmatrix} 0 \\ 0 \\ \frac{i\lambda}{4\rho\omega_R}(\tilde{x}\tilde{x}^* + \tilde{y}\tilde{y}^*) \end{bmatrix}. \quad (29)$$

This mean correction has a physical interpretation: the positive definite quantity  $\tilde{x}\tilde{x}^* + \tilde{y}\tilde{y}^* = |\tilde{x}|^2 + |\tilde{y}|^2$  is the squared radial position of the pendulum in the modulation variable. As the mean correction only has a component in the  $z$  coordinate, the initial states of  $\mathbf{u}(0)$  and  $\mathbf{w}(0)$  have the same  $x$  and  $y$  components. This allows for the mean corrected initial condition to be defined explicitly from the standard initial condition,  $\mathbf{u}_0 = [\hat{x}_0, \hat{y}_0, \hat{z}_0]^T$ , as,

$$\mathbf{w}(0) = \mathbf{u}_0 - \mathcal{L}^{-1}\mathbf{C}_\infty(\mathbf{u}_0) = \begin{bmatrix} \hat{x}_0 \\ \hat{y}_0 \\ \hat{z}_0 - \frac{\lambda}{4\rho^2\omega_R^2}(\hat{x}_0\hat{x}_0^* + \hat{y}_0\hat{y}_0^*) \end{bmatrix}. \quad (30)$$

### 3.3 Results

Parameters following (Lynch, 2003) of  $l_0 = 1.2, l = 1, \omega_R = \pi$  are used, with an initial condition vector of  $\mathbf{u}(0) = [0.04, 0.03427i/\pi, 0.08]$ . The simulations are run for a total time of 200 s. Explicit RK4 is used to solve (6) and (8) for the phase-averaged and mean corrected (with algorithm 2) methods respectively, using the operators in (25). A large timestep was of  $\Delta t = 0.5$  is used. Errors are measured as an L2 difference of the coordinate positions relative to a reference solution computed using RK4 and  $\Delta t = 0.01$ .

Errors at the best averaging window for each method are shown in Figure 1. The mean corrected method has a lower error at all resonance factors, so has improved accuracy for the directly resonant, near-resonant and out-of-resonance interaction settings of the swinging spring. This efficacy for a range of dynamical situations motivates the application of a mean correction in PDEs with a bilinear  $\mathcal{N}(\mathbf{u}, \mathbf{u})$  like the cases in sections 4 and 5, as these systems can be expanded as a sum of three-wave interactions of different frequencies (Embid & Majda, 1996; A. Peddle, 2018). The accuracy improvement is greater for interactions of  $\rho > 1.82$ , which highlights that the mean correction may have a larger impact for certain regimes of nonlinear dynamics.

The best averaging windows are identified from the lowest error of each method over a range of averaging windows separated by  $\Delta\zeta = 0.1$ . The existence of optimal averaging windows is shown in Peddle plots in Figure 2. The mean corrected method often has multiple minima in the swinging spring Peddle plots (Figure 2b); this feature is also present in the RSWEs for analogous plots over  $\eta_C$  (Figure 7b).

The effect of the mean correction can be observed when comparing the modulation variable spaces of both methods in Figure 3. An unaveraged modulation variable solution using (3) represents shows the ‘true’ modulation variable solution. This still contains small amplitude fluctuations, which the phase-averaged method seeks to reduce. This introduces an averaging error, which presents itself as a phase discrepancy in the modulation space, even at the best window for the phase-averaged method (Figure 3a). With a larger averaging window (Figure 3b), the phase-averaged solution is smoother but the phase errors are more prevalent, with the  $z$ -coordinate solution often being 180 degrees out of phase. The mean corrected method has a much lower

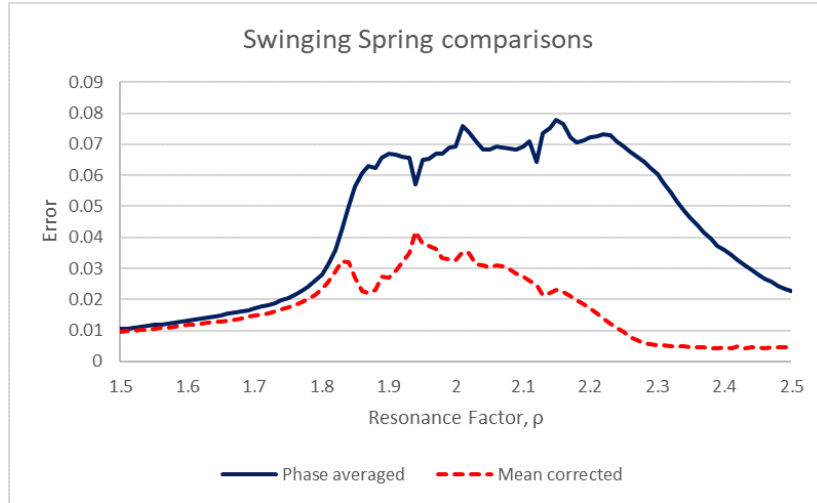
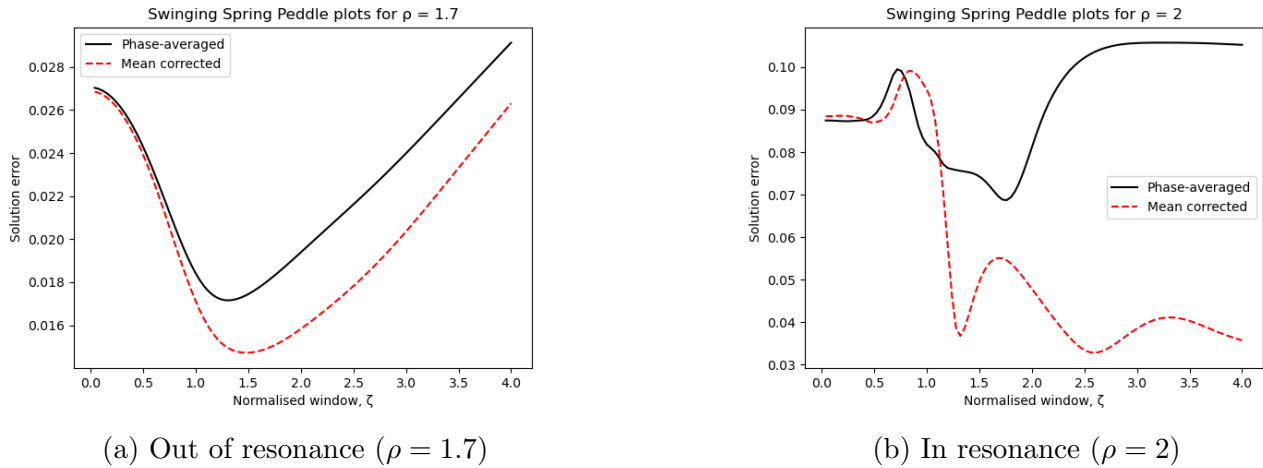


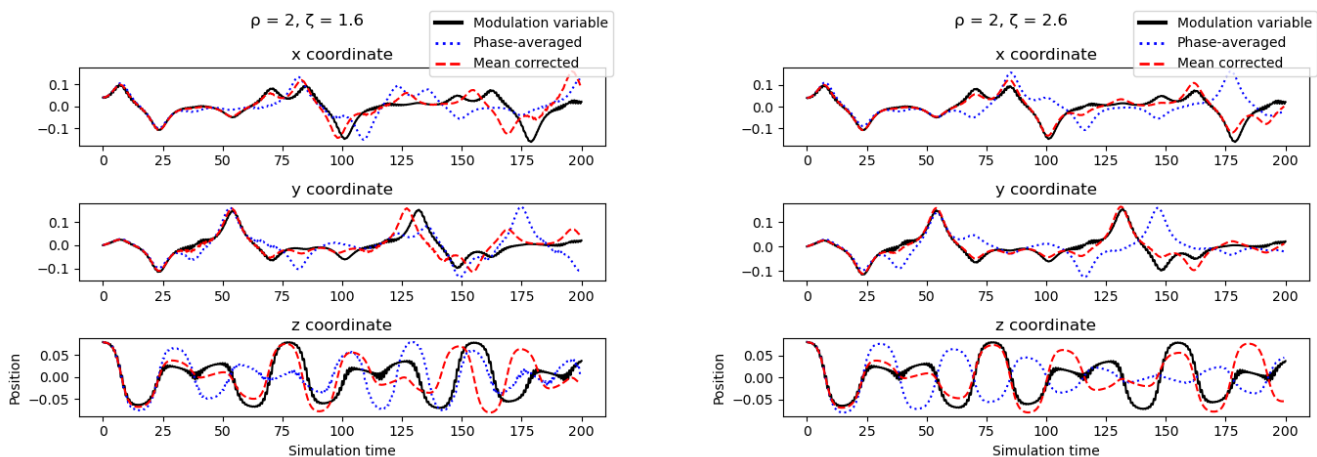
Figure 1: Errors of the phase-averaged (solid line) and mean corrected (dashed) methods for the swinging spring. The mean corrected method is more accurate for all the resonance factors examined, which models a range of in- and out-of-resonance interactions.



(a) Out of resonance ( $\rho = 1.7$ )

(b) In resonance ( $\rho = 2$ )

Figure 2: Peddle plots of the errors over normalised averaging window,  $\zeta = \eta/\Delta t$ . In an out-of-resonance case (a), there is a clear minimum in the error for each method, with the best window for the mean corrected method being slightly larger. For the directly resonant case (b), the mean corrected method again is best with a larger window, but there are also multiple local minima in the error.



(a) Best  $\zeta$  for the phase-averaged method

(b) Best  $\zeta$  for the mean corrected method

Figure 3: Comparing the unaveraged modulation variable solution ( $\mathbf{v}$ , solid line), with the modulation variables of the phase-averaged method ( $\bar{\mathbf{v}}$ , dotted) and mean corrected method ( $\bar{\mathbf{w}}$ , dashed). This is in the directly resonant state of  $\rho = 2$ . The modulation variable solutions in (a) use the best  $\zeta$  for the phase-averaged method, whilst (b) uses the best  $\zeta$  for the mean corrected method. The mean corrected method aligns better in the modulation space with its best averaging window in (b), whereas the phase-averaged method has considerable phase discrepancies, even in (a).

phase error with its best  $\eta^*$  in Figure 3b. Hence, the information in the mean correction increases the accuracy within the modulation variable space itself.

## 4 PDE System 1: One-dimensional Klein-Gordon-type PDE

### 4.1 Equations

We now turn to a PDE example of a one-dimensional Klein-Gordon-type (KG-type) equation. This is one of the simplest wave systems with purely oscillatory linear dynamics. We consider a quadratic nonlinearity,

$$\frac{\partial^2 u}{\partial t^2} - \alpha \frac{\partial^2 u}{\partial x^2} + \beta u + \gamma u^2 = 0. \quad (31)$$

A multiscale system can be generated with a specific choice of parameters  $\alpha, \beta, \gamma$ ,

$$\frac{\partial^2 u}{\partial t^2} + \frac{1}{\epsilon^2} \left( u - \frac{\partial^2 u}{\partial x^2} \right) = -u^2. \quad (32)$$

A linear dispersion relation of  $\omega = \pm\sqrt{1+k^2}$  can be identified from the spatial Fourier transform of (32). To obtain a first-order-in-time system with a Skew-Hermitian  $\mathcal{L}$ , we introduce variables of  $a = (\omega/\epsilon)u$ ,  $b = \frac{\partial u}{\partial t}$ . For a solution vector of  $\mathbf{u} = [a, b]^T$ , we have the following operators in Fourier space for a system in the standard form (1),

$$\mathcal{L} = \begin{bmatrix} 0 & -\omega \\ \omega & 0 \end{bmatrix}, \quad \mathcal{L}^{-1} = \begin{bmatrix} 0 & \frac{1}{\omega} \\ \frac{-1}{\omega} & 0 \end{bmatrix}, \quad \mathcal{N} = \left[ -\left(\frac{\epsilon}{\omega}a\right) \circledast \left(\frac{\epsilon}{\omega}a\right) \right], \quad (33)$$

where  $\circledast$  denotes a circular spatial convolution. In this standard form, the KG-type equation is both weakly nonlinear ( $\mathcal{N} \sim \mathcal{O}(\epsilon^2)$ ) and multiscale ( $\epsilon^{-1}\mathcal{L} \sim \mathcal{O}(\epsilon^{-1})$ ).

The eigenvalues of the linear operator are  $\pm i\omega$ , with the corresponding Fourier space matrix exponential only containing trigonometric terms,

$$e^{\pm \frac{t\mathcal{L}}{\epsilon}} = \begin{bmatrix} \cos\left(\frac{\omega t}{\epsilon}\right) & \mp \sin\left(\frac{\omega t}{\epsilon}\right) \\ \pm \sin\left(\frac{\omega t}{\epsilon}\right) & \cos\left(\frac{\omega t}{\epsilon}\right) \end{bmatrix}. \quad (34)$$

We consider an analytical mean correction (17), like was used for weakly nonlinear systems in (Tao, 2019), as well as a numerical mean correction (18). The details of the analytical mean correction, which is computed in Fourier space, are given in Appendix B. The numerical mean correction is computed using algorithm 2 with the simple, computationally cheap choice of  $\eta_C = \eta$ .

## 4.2 Results

A one-dimensional spatial domain of length  $[0, 2\pi]$  is used, with  $N_x = 32$  grid points and periodic boundary conditions. Gaussian initial conditions are applied as a perturbation to the  $a$  field, with a uniformly zero field for  $b$ , which corresponds to an initial rest state,

$$a(x, 0) = \exp\left(\frac{-(x - \pi)^2}{2}\right), \quad b(x, 0) = 0. \quad (35)$$

We use a pseudospectral method (Boyd, 2001; Canuto et al., 2007) for this system and the RSWEs in section 5. This allows the Fourier space operators (33) and analytical matrix exponential (34) to be used, as well as the analytical mean correction in Appendix B. The matrix exponential can also be applied in non-Fourier domains (T. S. Haut et al., 2016; Moler & Van Loan, 1978). The nonlinear term is computed using Fast Fourier Transforms to map the solution variables between physical and spectral space — this uses the cheaper multiplication operation instead of spatial convolutions. Using the operators in (33), an explicit RK4 scheme is applied to equation (6) for the phase-averaged method, with the number of kernel points being defined using (15) and  $\omega_{max} = \sqrt{1 + k_{max}^2}$ . algorithm 2 is used for the mean corrected method. A total simulation time of  $T_{max} = 20$  is used, with large timesteps in the range  $\Delta t \in [1, 3]$ . The error metric is an L1 difference in the  $a$  field relative to an unaveraged modulation variable RK4 solution (3) with  $\Delta t = 10^{-4}$ .

The initial condition for the mean corrected modulation variable is computed using algorithm 3 and  $C_{tol} = 10^{-10}$ . For these experiments  $\epsilon \in \{0.5, 0.1, 0.05, 0.01\}$  are examined. We compute the errors of both methods over a range of averaging windows separated by  $\Delta\zeta = 0.05$ . Different  $\eta^*$  are usually identified for all three methods, although these are identical for  $\epsilon = 0.01$  for all but the largest timestep.

Figure 4 shows that both implementations of the mean correction (analytical and numerical) have lower errors than the phase-averaged method, for the examined timesteps and values of  $\epsilon$ . The numerical mean correction has a lower error than the analytical for  $\epsilon \in \{0.1, 0.05\}$ . The largest  $\epsilon$  value of 0.5 sees the two methods performing similarly, with the analytical correction sometimes being more accurate. A possible reason for this may be the neglect of the  $\epsilon \frac{\partial}{\partial \mathbf{w}} (\mathcal{L}^{-1} \mathbf{C})$  term from (19), as the numerical correction has more variation, which increases the size of this term. For the fastest oscillation case of  $\epsilon = 0.01$ , the mean corrected methods differ by less than 2% relative to the phase-averaged error. This is due to the numerical mean correction tending to the analytical as  $\epsilon$  reduces. This is observable in visualisations of the mean corrections in physical space (Figure 5). The analytical mean correction has a near identical mean correction for all regimes except  $\epsilon = 0.5$ , whilst the numerical corrections are distinctly unique at each  $\epsilon$ . This

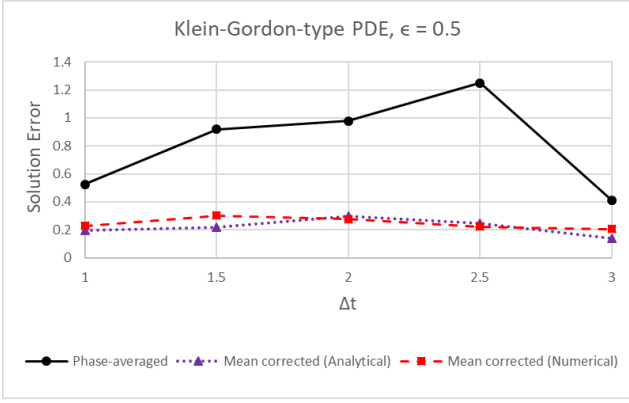
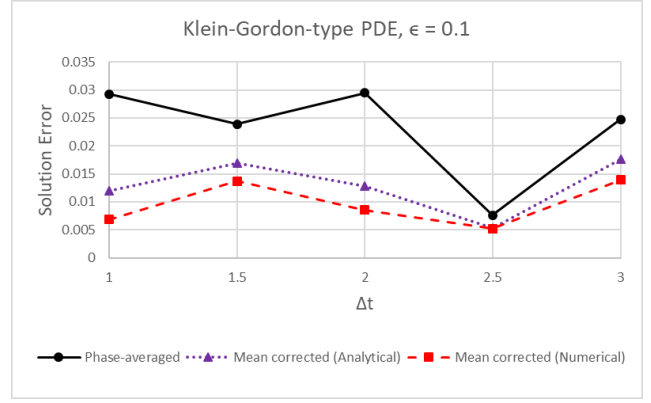
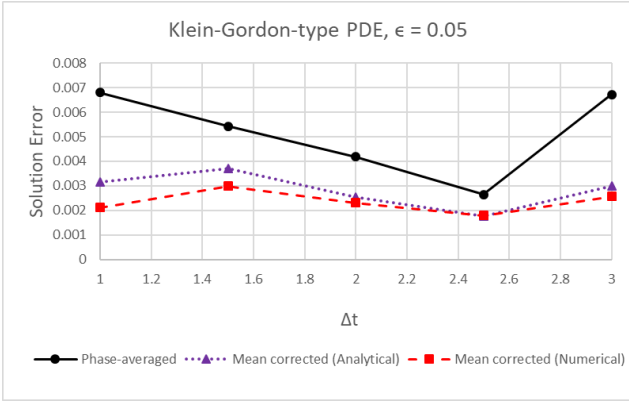
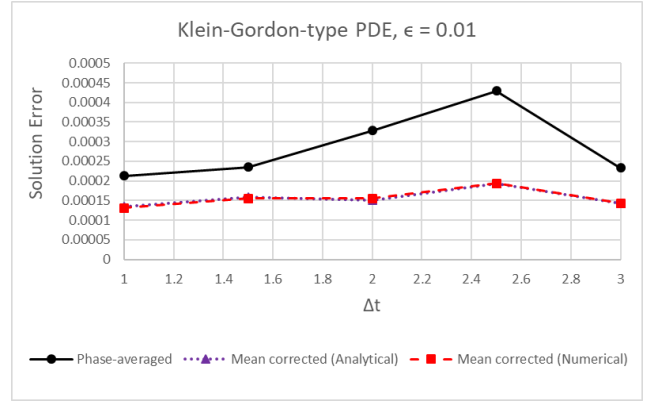
(a)  $\epsilon = 0.5$ (b)  $\epsilon = 0.1$ (c)  $\epsilon = 0.05$ (d)  $\epsilon = 0.01$ 

Figure 4: Errors for the phase-averaged (solid line), analytically mean corrected (dotted line), and numerically mean corrected (dashed line) methods in the KG-type system. The two mean corrected methods are more accurate than the phase-averaged one for all values of  $\epsilon$ . The numerical mean correction has a lower error than the analytical for  $\epsilon \in \{0.1, 0.05\}$ . At  $\epsilon = 0.01$  there is minimal difference between  $C_\infty$  and  $C$ , so both mean corrected methods perform similarly.

demonstrates how the finite averaging window of the numerical correction captures local variations in the mean of the oscillations. The analytical correction loses this with the complete removal of oscillations.

## 5 PDE System 2: One-dimensional Rotating Shallow Water Equations

### 5.1 Equations

We lastly demonstrate the mean corrected method in the one-dimensional Rotating Shallow Water Equations (RSWEs), which are a simplified system relevant for weather and climate applications. These equations were used to test other phase-averaged implementations in (T. Haut & Wingate, 2014; A. G. Peddle et al., 2019; Rosemeier et al., 2022).

The prognostic variables of the RSWEs include a two-dimensional fluid velocity,  $(u, v)$ , and

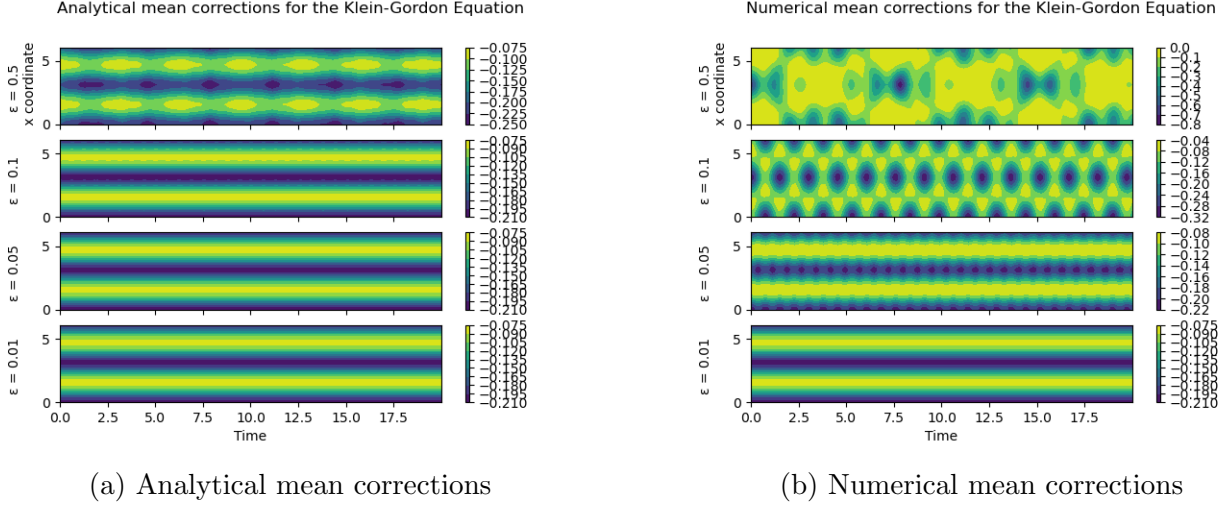


Figure 5: Visualisations of the underlying analytical and numerical mean corrections in the KG-type system; these are approximated in a large timestep solution. The best  $\eta_C$  for each method at  $\Delta t = 1$  is used to compute mean corrections from a small timestep unaveraged modulation variable ( $\mathbf{v}$ ) solution. The inverse Fourier transform is performed to give a physical (as opposed to spectral) space visualisation. Mean corrections from faster linear oscillations are shown moving down the page, with  $\epsilon \in \{0.5, 0.1, 0.05, 0.01\}$ . The analytical mean correction has a different profile for  $\epsilon = 0.5$ , but is visually indistinguishable in the other regimes. In contrast, the numerical mean correction has an observable variation between each  $\epsilon$  regime. This is a result of the finite  $\eta_C$  capturing different local mean dynamics depending on the oscillation frequency. At  $\epsilon = 0.01$ , the mean corrections are visually indistinguishable; this coincides with the two methods having similar accuracy.

a surface elevation,  $\eta_h$ , above the mean height of the fluid layer,  $H_0$ , e.g. (Salmon, 1996). To symmetrise the equations, we use a geopotential,  $\phi = \sqrt{g/H_0} \eta_h$ , where  $g$  is the gravitational force. These choices give the following equation set in one-dimension,

$$\frac{\partial u}{\partial t} + u \frac{\partial u}{\partial x} - fv + c \frac{\partial \phi}{\partial x} = 0, \quad (36a)$$

$$\frac{\partial v}{\partial t} + u \frac{\partial v}{\partial x} + fu = 0, \quad (36b)$$

$$\frac{\partial \phi}{\partial t} + c \frac{\partial u}{\partial x} + \frac{\partial}{\partial x}(u\phi) = 0, \quad (36c)$$

where  $f$  is a constant Coriolis force and  $c = \sqrt{gH}$  is the irrotational linear wave speed.

To express the RSWEs in the form of (1), we choose a scaling of  $f = c = 1/\epsilon$ . This value of  $\epsilon$  in the RSWEs measures the timescale separation between the linear and nonlinear operators. Representing this system in Fourier space, where  $\hat{\mathbf{u}} = [\hat{u}, \hat{v}, \hat{\phi}]^T$  are the spatially Fourier transformed variables, we have the following operators in the timescale separated form of (1),

$$\mathcal{L} = \begin{bmatrix} 0 & -1 & ik \\ 1 & 0 & 0 \\ ik & 0 & 0 \end{bmatrix}, \quad \mathcal{N} = \mathcal{F} \left\{ - \begin{bmatrix} u \frac{\partial u}{\partial x} \\ u \frac{\partial v}{\partial x} \\ \frac{\partial}{\partial x}(u\phi) \end{bmatrix} \right\}, \quad (37)$$

where  $\mathcal{F}$  denotes the spatial Fourier transform.



The linear dispersion relation of  $\mathcal{L}$  in (37) is  $\omega = \pm\alpha\sqrt{1+k^2}$ , with  $\alpha \in \{-1, 0, 1\}$  denoting the dispersion relation branches. The fast modes of  $\alpha = \pm 1$  correspond to inertia-gravity waves and have the same dispersion relation as the modes of the KG-type equation. Additionally, there is a slow mode of  $\omega = 0$  corresponding to Rossby waves. The speed of these waves is identically zero as a result of a constant Coriolis force. A further consequence is that  $\mathcal{L}$  is singular and  $\mathcal{L}^{-1}$  is undefined. As such, the Moore-Penrose pseudoinverse,  $\mathcal{L}^+$ , is used in place of the regular inverse. This means that  $\mathcal{L}\mathcal{L}^+ \neq I$ ,

$$\mathcal{L}^+ = \begin{bmatrix} 0 & \frac{1}{\psi^2} & \frac{-ik}{\psi^2} \\ \frac{-1}{\psi^2} & 0 & 0 \\ \frac{-ik}{\psi^2} & 0 & 0 \end{bmatrix}, \quad \mathcal{L}\mathcal{L}^+ = \begin{bmatrix} 1 & 0 & 0 \\ 0 & \frac{1}{\psi^2} & \frac{-ik}{\psi^2} \\ 0 & \frac{ik}{\psi^2} & \frac{k^2}{\psi^2} \end{bmatrix}, \quad (38)$$

where  $\psi = \sqrt{1+k^2}$ .

The matrix exponential for this system can be written analytically in Fourier Space,

$$e^{\pm \frac{t}{\epsilon} \mathcal{L}} = \begin{bmatrix} \cos(\frac{\psi t}{\epsilon}) & \mp \frac{1}{\psi} \sin(\frac{\psi t}{\epsilon}) & \pm \frac{ik}{\psi} \sin(\frac{\psi t}{\epsilon}) \\ \pm \frac{1}{\psi} \sin(\frac{\psi t}{\epsilon}) & \frac{1}{\psi^2} (k^2 + \cos(\frac{\psi t}{\epsilon})) & \frac{ik}{\psi^2} (1 - \cos(\frac{\psi t}{\epsilon})) \\ \pm \frac{ik}{\psi} \sin(\frac{\psi t}{\epsilon}) & \frac{ik}{\psi^2} (\cos(\frac{\psi t}{\epsilon}) - 1) & \frac{1}{\psi^2} (1 + k^2 \cos(\frac{\psi t}{\epsilon})) \end{bmatrix}. \quad (39)$$

Dissipation is required for stabilisation purposes and is applied in the form of a  $(\nabla^2)^2$  hyperviscosity,

$$\mathcal{D} = \begin{bmatrix} -\mu k^4 & 0 & 0 \\ 0 & -\mu k^4 & 0 \\ 0 & 0 & -\mu k^4 \end{bmatrix}. \quad (40)$$

We use the following equations for the mean corrected method,

$$\mathbf{u} = e^{-\frac{t}{\epsilon} \mathcal{L}} \mathbf{w} + \epsilon \mathcal{L}^+ \mathbf{C}, \quad (41a)$$

$$\frac{\partial \bar{\mathbf{w}}}{\partial t} = \left\langle e^{\frac{t+s}{\epsilon} \mathcal{L}} \left[ \mathcal{N}^* \left( e^{-\frac{t+s}{\epsilon} \mathcal{L}} \bar{\mathbf{w}}(t) + \epsilon \mathcal{L}^+ \mathbf{C} \right) - \mathcal{L} \mathcal{L}^+ \mathbf{C} \right] \right\rangle_s, \quad (41b)$$

$$\bar{\mathbf{w}}(0) = \mathbf{u}_0 - \epsilon \mathcal{L}^+ \mathbf{C}(\bar{\mathbf{w}}(0)), \quad (41c)$$

where  $\mathcal{N}^*(\mathbf{u}) = \mathcal{N}(\mathbf{u}) + \mathcal{D}\mathbf{u}$  is the nonlinear vector with added dissipation.

## 5.2 Results

We consider initial conditions of a Gaussian perturbation to the geopotential height field, at a state of rest,

$$u(x, 0) = 0, \quad v(x, 0) = 0, \quad \phi(x, 0) = \exp\left(\frac{-(x-\pi)^2}{2}\right). \quad (42)$$

A spatially periodic domain of size  $[0, 2\pi]$  is used with  $N_x = 32$  grid points. The initial condition for the modulation variable is computed with the fixed-point iteration of algorithm 3 and  $C_{tol} = 10^{-10}$ . A hyperviscosity coefficient of  $\mu = 10^{-4}$  is used. The phase-averaged solution is computed using (6) with the dissipation-stabilised  $\mathcal{N}^*$  in place of  $\mathcal{N}$ . The mean corrected method applies algorithm 2 to (41). The use of a pseudospectral method allows the analytical matrix exponential (39) to be used. Alternate matrix exponential constructions for the RSWEs include rational approximations, e.g. (T. S. Haut et al., 2016; Schreiber et al., 2018), or Chebyshev

approximation (Yamazaki et al., 2023). We present results for a total simulation time of  $T_{max} = 10$ . The error metric is an L2 combination of pointwise differences in each solution component relative to a reference RK4 solution that solves (3) with  $\Delta t = 10^{-4}$ .

The phase-averaged and numerically mean corrected methods errors are compared at timescale separations of  $\epsilon \in \{0.5, 0.1, 0.05, 0.01, 0.001\}$  in Figure 6. The numerical mean correction enables greater accuracy in the cases with sufficiently fast oscillations ( $\epsilon \geq 0.1$ ). Although at certain timesteps the mean correction has a minimal effect (e.g.  $\Delta t = 0.1, 0.2$  for  $\epsilon = 0.01$ ) it crucially does no worse than standard phase-averaging for these configurations. This is consistent with this proven property for the weakly nonlinear, classically time averaged case (Section 2.1, (Tao, 2019)). The mean correction continues to provide accuracy improvements at very large timescale separations ( $\epsilon = 0.001$ ). The mean corrected method does not perform better for the timescale separation of  $\epsilon = 0.5$ , and one possibility for this is neglecting the  $\mathcal{O}(\epsilon)$  term in (19).

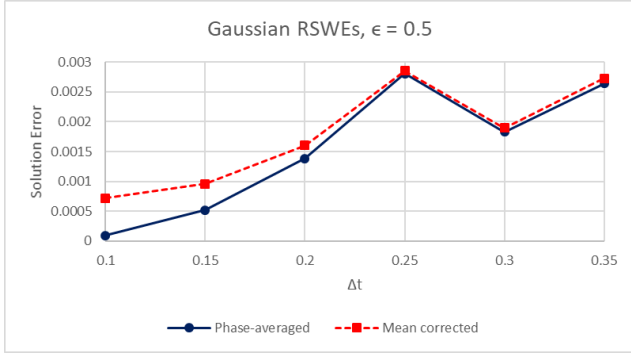
The numerically mean corrected method requires the selection of an  $(\eta, \eta_C)$  pairing. Using the same  $\eta^*$  as the phase-averaged method is an effective choice (like with the KG-type system) so we only examine errors over different  $\eta_C$  values for the mean corrected method. This does not guarantee optimality over the full two-dimensional  $(\eta, \eta_C)$  space, but is cheaper computationally and still demonstrates accuracy improvements. The  $(\eta^*, \eta_C^*)$  selection procedure is,

- i) Apply the phase-averaged method over a range of  $\zeta = \eta/\Delta t$  values to find the window with lowest error,  $\eta^*$ . For the RSWEs, increments of  $\Delta\zeta = 0.05$  are used.
- ii) Using the  $\eta^*$  value found in i), apply the mean corrected method over a range of  $\eta_C$  values to identify the numerical mean correction window with lowest error,  $\eta_C^*$ . For the RSWEs, increments of  $\Delta\eta_C = \epsilon$  are used.

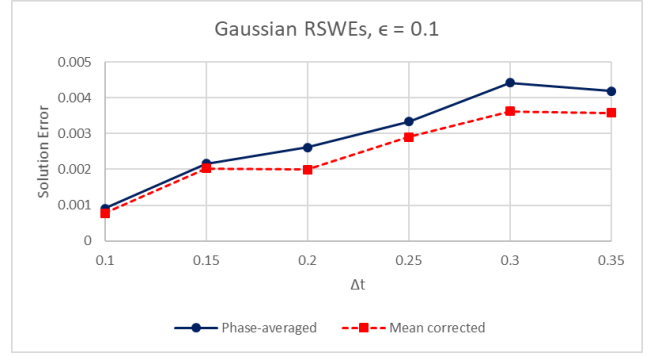
The size of  $\eta_C^*$  is dependent on the timescale separation, as shown in Figure 7a. As  $\epsilon$  reduces, a smaller averaging window is needed to capture a similar number of linear oscillations in the support of  $\mathcal{K}_C$ . As such, the computation of the mean correction scales well to larger timescale separations, as the required  $K_s$  for the  $\langle \cdot \rangle_r$  operation does not increase with a smaller  $\epsilon$ , whilst  $K$  does for the standard  $\langle \cdot \rangle_s$  phase-average (15).

The errors for the mean corrected method over  $\eta_C$  differ from those seen in the PDE Peddle plots over  $\eta$ , in that there are multiple local minima as opposed to a single optima (Figure 7b). The locations of these minima are similar over a range of  $\Delta t$ , so unlike the choice of  $\eta^*$ , the mean correction window selection is less dependent on the timestep size. This is because the mean correction is only an average quantity of the current time-solution,  $\mathbf{w}(t)$ , so its computation does not use the size of  $\Delta t$ . A larger timestep can mean that a local minima at a smaller  $\eta_C$  value is best, as is the case at  $\epsilon = 0.1$  in Figure 7b.

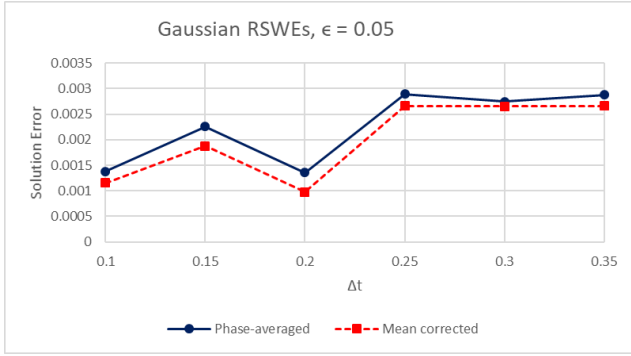
The components of the mean correction in physical space are visualised in Figure 8, for two values of  $\eta_C$  and  $\epsilon = 0.05$ . Similar mean dynamics are observed in both cases, with two periods across the spatial dimension in the  $u$  component. This pattern results from a single Gaussian bump in the initial condition evolving with a quadratically nonlinear interaction, i.e., in the  $u$  component  $\mathcal{N}_u = -u \frac{\partial u}{\partial x}$ . A smaller  $\eta_C = 0.35$  in Figure 8b, compared to  $\eta_C = 1.35$  in Figure 8a, allows greater variation in the mean correction over time. When using a larger timestep, there is a smaller variation in the error magnitude and the mean correction with a smaller  $\eta_C$  often leads to greater accuracy, as observed in Figure 7b.



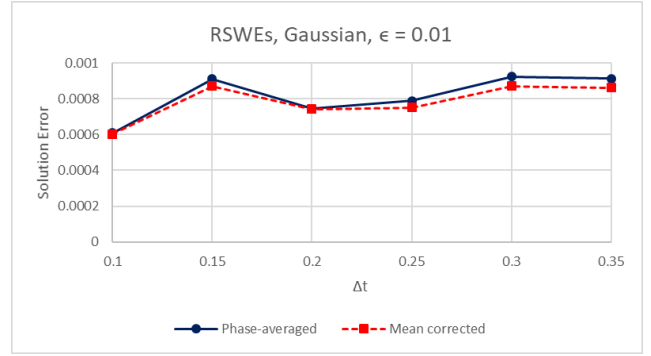
(a)  $\epsilon = 0.5$



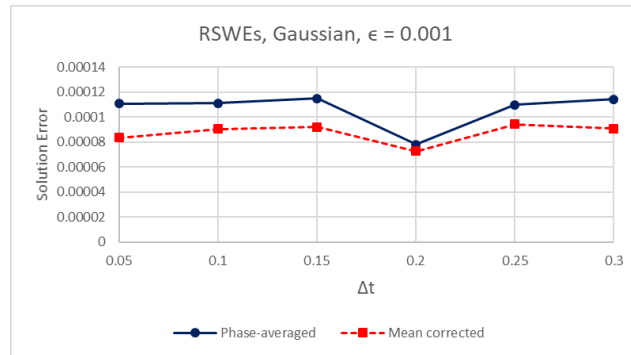
(b)  $\epsilon = 0.1$



(c)  $\epsilon = 0.05$

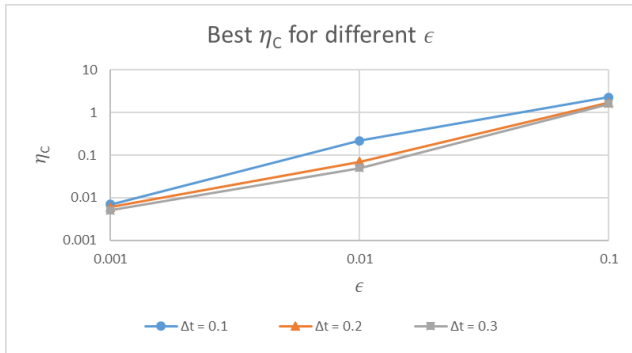


(d)  $\epsilon = 0.01$

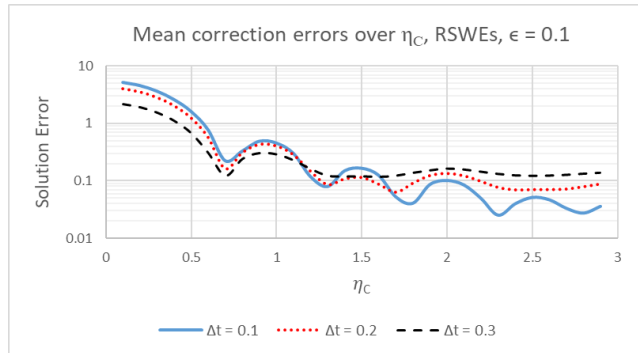


(e)  $\epsilon = 0.001$

Figure 6: Phase-averaged (solid line) and mean corrected (dashed) errors for the RSWEs. Accuracy improvements with the mean correction are observed in the regimes with  $\epsilon \geq 0.1$ . The mean correction improves the accuracy to a lesser degree in the  $\epsilon = 0.01$  case, but crucially, does no worse than standard phase-averaging. For this implementation in the RSWEs, the linear oscillations with  $\epsilon = 0.5$  are insufficiently fast for the mean correction to be effective.



(a) Best  $\eta_C$  for different  $\epsilon$



(b) Mean corrected errors over  $\eta_C$ , with  $\epsilon = 0.1$

Figure 7: Investigating the selection of the best  $\eta_C$  for the RSWEs. In (a), the mean correction window with the lowest error,  $\eta_C^*$ , is plotted against timescale separations of  $\epsilon \in \{0.1, 0.01, 0.001\}$  for different timestep sizes. There is a relatively linear scaling between  $\eta_C^*$  and  $\epsilon$  on these logarithmic axes. This reflects that the size of  $\eta_C^*$  adjusts to consider a similar number of linear oscillations within the support of  $\mathcal{K}_C$ . In (b), the local minimal error locations are similar with different timestep size, although a larger  $\Delta t$  leads to less variation in the error over  $\eta_C$ . The best  $\eta_C$  generally reduces with larger timestep: the third local minima around  $\eta_C = 2.7$  was best for  $\Delta t = 0.1$ , whilst the second local minima of  $\eta_C = 1.7$  was best for  $\Delta t \in \{0.2, 0.3\}$ .

## 6 Discussion

This paper introduced a modified mapping with a mean correction term to improve phase-averaging accuracy in oscillatory, multiscale, differential equations. Examples with an analytical mean correction, which enabled accuracy improvements with a weak nonlinearity (Tao, 2019), demonstrate that the mean correction is also applicable in multiscale systems. We provided algorithms for a numerical mean correction and timestepping method that uses a finite averaging window; this extends the phase-averaging framework of (A. G. Peddle et al., 2019). Improved accuracy with this mean corrected method is demonstrated in the one-dimensional RSWEs.

With a finite phase-average, the experiments in the two PDE systems show that the best numerical mean correction also uses a finite window size,  $\eta_C^*$ . This quantifies a time interval that is long enough to obtain a mean value of the nonlinear oscillations, whilst retaining pertinent local variation. This is analogous to how the finite time interval of a phase-average preserves the low-frequency dynamics and interactions; these are missing from a classical time average which has a cancellation of all oscillations.

Work is ongoing on developing a more efficient algorithm that precomputes a matrix exponential of  $\exp(\pm\Delta t\mathcal{L})$  before the timestepping routine, as opposed to  $\exp(\pm t\mathcal{L})$  at each time step. Examples of this approach include Lawson-RK methods, such as the fourth-order version used in (Yamazaki et al., 2023), or a Strang-split method, as was used in (T. Haut & Wingate, 2014). Other interesting additions to this method include an optimisation algorithm to more efficiently select  $\eta$  and  $\eta_C$ , and extending the improved accuracy into slower oscillation regimes, i.e.  $\epsilon \rightarrow 1$ . Additionally, we will test the new mapping as a modified coarse solver in the oscillatory parareal method of (A. G. Peddle et al., 2019). As the mean correction can be computed in parallel, like the phase-averaging procedure, it should provide a cheap modification to the coarse solver to improve its accuracy.

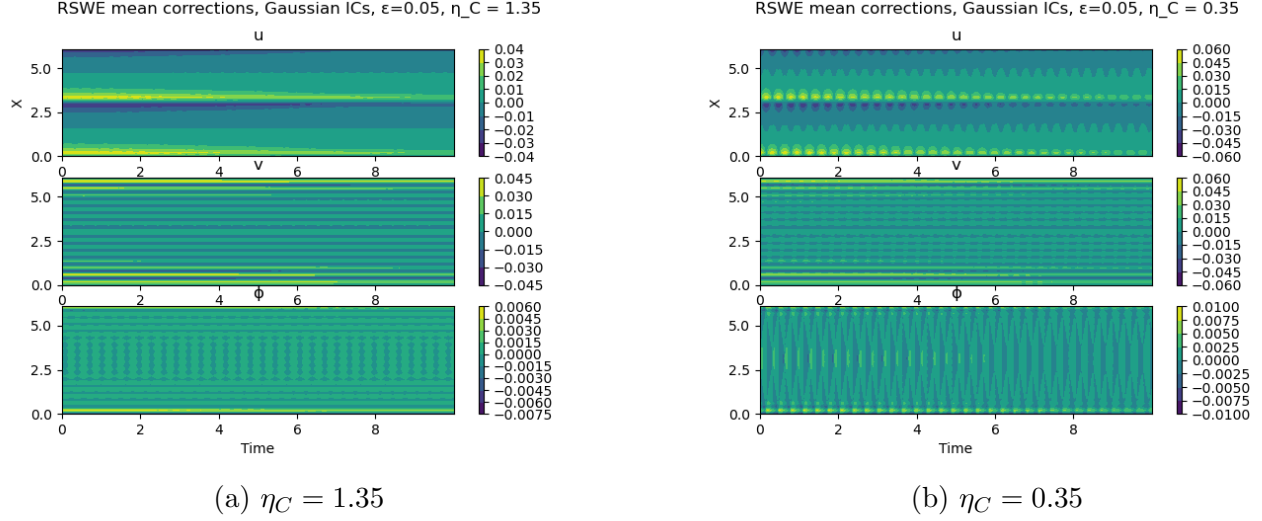


Figure 8: Visualisations of each component of the RSWEs mean correction using two different  $\eta_C$  values, at  $\epsilon = 0.05$ . These are computed from  $\langle \cdot \rangle_r$  averages of a fine timestep  $\mathbf{v}$  solution and transformed into physical space (analogously to Figure 5). The larger  $\eta_C = 1.35$  in (a) is best for the smaller timestep of  $\Delta t = 0.1$ ; this corresponds to the third local minima in the error over  $\eta_C$ , like in Figure 7b. This larger window has a smoother evolution of the mean correction over time. The smaller  $\eta_C = 0.35$  in (b) is best for the larger timestep of  $\Delta t = 0.2$  and corresponds to the first minima in the error over  $\eta_C$ . This smaller averaging window allows for more local variation to be captured in  $\mathbf{C}(t)$ . This is seen through shorter timescale oscillations in the  $u$  component of (b) which are smoothed out in (a). The magnitude of each mean correction component reduces with a larger  $\eta_C$ , as there is more cancellation of oscillations.

## Appendix A: Cancellation of oscillations example for the swinging spring $\mathbf{C}_\infty$

Consider the first term in the  $x$ -component of  $\mathcal{N}(e^{-t\mathcal{L}}\mathbf{w})$  in (28),

$$\frac{i\lambda}{4\omega_R} A \tilde{x} \tilde{z} = \frac{i\lambda}{4\omega_R} e^{-i(\rho+1)\omega_R t} \tilde{x}(t) \tilde{z}(t). \quad (43)$$

Applying (17) to obtain the mean value over all time,

$$\lim_{T_C \rightarrow \infty} \frac{1}{T_C} \int_{r=0}^{T_C} \frac{i\lambda}{4\omega_R} e^{-i(\rho+1)\omega_R(t+r)} \tilde{x}(t) \tilde{z}(t) dr. \quad (44)$$

Phase-averaging is performed at a fixed solution value, allowing most terms to be taken outside of the integral,

$$\frac{i\lambda}{4\omega_R} e^{-i(\rho+1)\omega_R t} \tilde{x}(t) \tilde{z}(t) \lim_{T_C \rightarrow \infty} \frac{1}{T_C} \int_0^{T_C} e^{-i(\rho+1)\omega_R r} dr. \quad (45)$$

This integral evaluates to zero by the following property of complex exponentials,

$$\lim_{T_C \rightarrow \infty} \frac{1}{T_C} \int_0^{T_C} e^{i\phi t} dt = \begin{cases} 0, & \text{if } \phi \neq 0, \\ 1, & \text{if } \phi = 0. \end{cases} \quad (46)$$

Every term in (28) with a complex exponential component ( $A, B, C, D, E, F$ ) will have this cancellation of oscillations, resulting in a zero mean value and no contribution to  $\mathbf{C}_\infty$ .

## Appendix B: KG-type equation analytical mean correction

We begin by expressing the Fourier space nonlinear operator (33),  $\mathcal{N} = [\mathcal{N}_a, \mathcal{N}_b]^T$ , in terms of the mean corrected modulation variable,  $\mathbf{w} = [c, d]^T$ , using a mapping of the matrix exponential (34),

$$\mathcal{N}\left(e^{-\frac{t\mathcal{L}}{\epsilon}}\mathbf{w}\right) = \begin{bmatrix} 0 \\ -\left(c\frac{\epsilon}{\omega}\cos\left(\frac{\omega t}{\epsilon}\right) + d\frac{\epsilon}{\omega}\sin\left(\frac{\omega t}{\epsilon}\right)\right) \otimes \left(c\frac{\epsilon}{\omega}\cos\left(\frac{\omega t}{\epsilon}\right) + d\frac{\epsilon}{\omega}\sin\left(\frac{\omega t}{\epsilon}\right)\right) \end{bmatrix}, \quad (47)$$

where  $\otimes$  are spatial circular convolutions, defined in its discrete form for any two length  $N$  arrays,  $a$  and  $b$ ,

$$g = a \otimes b \quad \rightarrow \quad g_i = \frac{1}{N} \sum_{j=0}^{N-1} a_j b_{(i-j) \bmod N}. \quad (48)$$

We can expand the nonzero nonlinear component as  $\mathcal{N}_b = \mathcal{N}^I + \mathcal{N}^{II} + \mathcal{N}^{III} + \mathcal{N}^{IV}$ , as  $\otimes$  distributes over addition,

$$\begin{aligned} \mathcal{N}^I &= -\left(c\frac{\epsilon}{\omega}\cos\left(\frac{\omega t}{\epsilon}\right)\right) \otimes \left(c\frac{\epsilon}{\omega}\cos\left(\frac{\omega t}{\epsilon}\right)\right), \\ \mathcal{N}^{II} &= -\left(c\frac{\epsilon}{\omega}\cos\left(\frac{\omega t}{\epsilon}\right)\right) \otimes \left(d\frac{\epsilon}{\omega}\sin\left(\frac{\omega t}{\epsilon}\right)\right), \\ \mathcal{N}^{III} &= -\left(d\frac{\epsilon}{\omega}\sin\left(\frac{\omega t}{\epsilon}\right)\right) \otimes \left(c\frac{\epsilon}{\omega}\cos\left(\frac{\omega t}{\epsilon}\right)\right), \\ \mathcal{N}^{IV} &= -\left(d\frac{\epsilon}{\omega}\sin\left(\frac{\omega t}{\epsilon}\right)\right) \otimes \left(d\frac{\epsilon}{\omega}\sin\left(\frac{\omega t}{\epsilon}\right)\right). \end{aligned} \quad (49)$$

The mean correction can be decomposed into averages of each component of  $\mathcal{N}_b$  such that  $C^i = \langle \mathcal{N}^i \rangle_r$ . For an analytical mean correction, we evaluate each term in (49) in the limit of  $T_C \rightarrow \infty$  by applying (17). We then use the following property of trigonometric integration,

$$\lim_{T_C \rightarrow \infty} \frac{1}{T_C} \int_0^{T_C} \cos\left(\frac{\omega_a t}{\epsilon}\right) \cos\left(\frac{\omega_b t}{\epsilon}\right) dt = \begin{cases} \frac{1}{2}, & \text{if } \omega_a = \omega_b, \\ 0, & \text{if } \omega_a \neq \omega_b, \end{cases} \quad (50)$$

$$\lim_{T_C \rightarrow \infty} \frac{1}{T_C} \int_0^{T_C} \cos\left(\frac{\omega_a t}{\epsilon}\right) \sin\left(\frac{\omega_b t}{\epsilon}\right) dt = 0, \forall \omega_a, \omega_b, \quad (51)$$

$$\lim_{T_C \rightarrow \infty} \frac{1}{T_C} \int_0^{T_C} \sin\left(\frac{\omega_a t}{\epsilon}\right) \cos\left(\frac{\omega_b t}{\epsilon}\right) dt = 0, \forall \omega_a, \omega_b, \quad (52)$$

$$\lim_{T_C \rightarrow \infty} \frac{1}{T_C} \int_0^{T_C} \sin\left(\frac{\omega_a t}{\epsilon}\right) \sin\left(\frac{\omega_b t}{\epsilon}\right) dt = \begin{cases} \frac{1}{2}, & \text{if } \omega_a = \omega_b, \\ -\frac{1}{2}, & \text{if } \omega_a = -\omega_b, \\ 0, & \text{if } |\omega_a| \neq |\omega_b|. \end{cases} \quad (53)$$

By (51), (52),  $C^{II}$  and  $C^{III}$  will have a mean value of zero in the  $T_C \rightarrow \infty$  limit.  $C^I$  and  $C^{IV}$  will have a nonzero contribution to the analytical mean correction where  $|\omega_a| = |\omega_b|$  (53). Since the KG-type dispersion relation of  $\omega(k) = \sqrt{1+k^2}$  is an even function,  $\omega(k) = \omega(-k)$  and whenever two wavenumbers are of equal magnitude their frequencies will be the same. This leaves the following analytical mean correction,  $\mathbf{C}_\infty = [0, C^b]^T$ ,  $C^b = C^I + C^{IV}$ , where

$$C_i^I = \begin{cases} \frac{1}{2N_x} \sum_{j=0}^{N_x-1} \frac{c_j c_{-j \bmod N}}{\omega_j^2}, & \text{for } i = 0, \\ \frac{1}{2N_x} \left( \frac{c_{i/2}^2}{\omega_{i/2}^2} + \frac{c_{(i+N_x)/2}^2}{\omega_{(i+N_x)/2}^2} \right), & \text{for } i \text{ even}, \\ 0, & \text{for } i \text{ odd}, \end{cases} \quad (54)$$

$$C_i^{IV} = \begin{cases} \frac{1}{2N_x} \sum_{j=0}^{N_x-1} \frac{d_j d_{-j \bmod N}}{\omega_j^2}, & \text{for } i = 0, \\ \frac{1}{2N_x} \left( \frac{d_{i/2}^2}{\omega_{i/2}^2} + \frac{d_{(i+N_x)/2}^2}{\omega_{(i+N_x)/2}^2} \right), & \text{for } i \text{ even}, \\ 0, & \text{for } i \text{ odd}. \end{cases} \quad (55)$$

## References

- Babin, A., Mahalov, A., & Nicolaenko, B. (1998). On nonlinear baroclinic waves and adjustment of pancake dynamics. *Theoretical Computational Fluid Dynamics*, 11(3/4), 215–235.
- Babin, A., Mahalov, A., Nicolaenko, B., & Zhou, Y. (1997). On the asymptotic regimes and the strongly stratified limit of rotating Boussinesq equations. *Theoretical Computational Fluid Dynamics*, 9(3/4), 223–251.
- Bao, L., Klöforn, R., & Nair, R. D. (2015). Horizontally explicit and vertically implicit (hevi) time discretization scheme for a discontinuous galerkin nonhydrostatic model. *Monthly Weather Review*, 143(3), 972–990.
- Bauer, W., Cotter, C., & Wingate, B. (2022). Higher order phase averaging for highly oscillatory systems. *Multiscale Modeling & Simulation*, 20(3), 936–956.
- Bogoliubov, N. N., & Mitropolsky, Y. A. (1961). *Asymptotic Methods in the Theory of Non-linear Oscillations*. Gordon; Breach.
- Boyd, J. P. (2001). *Chebyshev and fourier spectral methods*. Courier Corporation.
- Butcher, J. C. (2016). *Numerical methods for ordinary differential equations*. John Wiley & Sons.
- Canuto, C., Hussaini, M., Quarteroni, A., & Zang, T. (2007). *Spectral methods: Fundamentals in single domains*. Springer Science & Business Media.
- Dullin, H., Giacobbe, A., & Cushman, R. (2004). Monodromy in the resonant swing spring. *Physica D: Nonlinear Phenomena*, 190(1-2), 15–37.
- Embid, P., & Majda, A. (1996). Averaging over fast gravity waves for geophysical flows with arbitrary potential vorticity. *Communications in Partial Differential Equations*.
- Embid, P., & Majda, A. (1998). Low Froude number limiting behaviour for stably stratified flow with small or finite rossby numbers. *Communications in Partial Differential Equations*.
- Engquist, B., & Tsai, Y.-H. (2005). Heterogeneous multiscale methods for stiff ordinary differential equations. *Mathematics of computation*, 74(252), 1707–1742.
- Giraldo, F. X., Kelly, J. F., & Constantinescu, E. M. (2013). Implicit-explicit formulations of a three-dimensional nonhydrostatic unified model of the atmosphere (numa). *SIAM Journal on Scientific Computing*, 35(5), B1162–B1194.
- Haut, T., & Wingate, B. (2014). An asymptotic parallel-in-time method for highly oscillatory PDEs. *SIAM Journal on Scientific Computing*, 36(2), A693–A713.

- Haut, T. S., Babb, T., Martinsson, P., & Wingate, B. (2016). A high-order time-parallel scheme for solving wave propagation problems via the direct construction of an approximate time-evolution operator. *IMA Journal of Numerical Analysis*, *36*(2), 688–716.
- Holm, D. D., & Lynch, P. (2002). Stepwise precession of the resonant swinging spring. *SIAM Journal on Applied Dynamical Systems*, *1*(1), 44–64.
- Hult, J. (2007). A fourth order runge-kutta method in the interaction picture method for simulating supercontinuum generation in optical fibres. *Journal of Lightwave Technology*.
- Jones, D., Mahlov, A., & Nicolaenko, B. (1999). A numerical study of an operator splitting method for rotating flows with large ageostrophic initial data. *Theoretical and Computational Fluid Dynamics*.
- Klainerman, S., & Majda, A. J. (1981). Singular limits of quasilinear hyperbolic systems with large parameters and the incompressible limit of compressible fluids. *Communications in Pure and Applied Mathematics*, *34*(4), 481–524.
- Lynch, P. (2002). Resonant motions of the three-dimensional elastic pendulum. *International Journal of Non-linear Mechanics*.
- Lynch, P. (2003). Resonant rossby wave triads and the swinging spring. *Bulletin of the American Meteorological Society*, *84*(5), 605–616.
- Mengaldo, G., Wyszogrodzki, A., Diamantaki, M., Lock, S., Giraldo, F., & Wedi, N. (2018). Current and emerging time-integration strategies in global numerical weather and climate prediction. *Archives of Computational Methods in Engineering*.
- Moler, C., & Van Loan, C. (1978). Nineteen dubious ways to compute the exponential of a matrix. *SIAM review*, *20*(4), 801–836.
- Peddle, A. (2018). *Components of nonlinear oscillation and optimal averaging for stiff pdes*. University of Exeter.
- Peddle, A. G., Haut, T., & Wingate, B. (2019). Parareal convergence for oscillatory pdes with finite time-scale separation. *SIAM Journal on Scientific Computing*, *41*(6), A3476–A3497.
- Penrose, R. (1955). A generalized inverse for matrices. *Mathematical proceedings of the Cambridge philosophical society*, *51*(3), 406–413.
- Ritchie, H., Temperton, C., Simmons, A., Hortal, M., Davies, T., Dent, D., & Hamrud, M. (1995). Implementation of the semi-lagrangian method in a high-resolution version of the ecmwf forecast model. *Monthly Weather Review*, *123*(2), 489–514.
- Rosemeier, J., Haut, T., & Wingate, B. (2022). Multi-level parareal algorithm with averaging. *arXiv preprint arXiv:2211.17239*.
- Salmon, R. (1996). *Lectures on geophysical fluid dynamics*. Oxford University Press.
- Sanders, J. A., Verhulst, F., & Murdock, J. (2007). *Averaging methods in nonlinear dynamical systems* (Vol. 59). Springer.
- Schochet, S. (1992). Fast singular limits of hyperbolic pdes. *Journal of Differential Equations*.
- Schreiber, M., Peixoto, P. S., Haut, T., & Wingate, B. (2018). Beyond spatial scalability limitations with a massively parallel method for linear oscillatory problems. *The International Journal of High Performance Computing Applications*, *32*(6), 913–933.
- Staniforth, A., & Côté, J. (1991). Semi-lagrangian integration schemes for atmospheric models—a review. *Monthly weather review*, *119*(9), 2206–2223.
- Tao, M. (2019). Simply improved averaging for coupled oscillators and weakly nonlinear waves. *Communications in Nonlinear Science and Numerical Simulation*, *71*, 1–21.
- Temperton, C., & Staniforth, A. (1987). An efficient two-time-level semi-lagrangian semi-implicit integration scheme. *Quarterly Journal of the Royal Meteorological Society*, *113*(477), 1025–1039.



- Weller, H., Lock, S.-J., & Wood, N. (2013). Runge–kutta imex schemes for the horizontally explicit/vertically implicit (hevi) solution of wave equations. *Journal of Computational Physics*, *252*, 365–381.
- Yamazaki, H., Cotter, C. J., & Wingate, B. A. (2023). Time parallel integration and phase averaging for the nonlinear shallow water equations on the sphere. *Quarterly Journal of the Royal Meteorological Society*.